SUPPLEMENTARY METHODS

Landslide Volume Estimation

We use a survey of landslides triggered by Typhoon Morakot (Marc et al., 2018) to estimate volume of hillslope material released during Typhoon Morakot. This survey mapped landslide area from remotely sensed data and does not differentiate between landslide source area and runout area. Empirical relationships between landslide area and landslide volume require knowledge of landslide source area. To estimate landslide volume from scar area, we separate soil and bedrock landslides, using a value of 10^5 m^2 as the cutoff. We assume a landslide scar to source ratio of 1.1 for the smaller landslides, and a ratio of 1.9 for larger bedrock landslides (Larsen et al., 2010). We estimate volume of landslide material using the relationship $V = \alpha A^{\gamma}$ where V is volume of landslide material, A is landslide source area, and α and γ are empirically derived constants. The constant γ is equal to 1.35 ± 0.01 or 1.332 ± 0.005, and $\log_{10}(\alpha)$ = -0.836 ± 0.015 or $\log_{10}(\alpha)$ = -0.73 ± 0.06 for shallow soil and deep bedrock landslides, respectively (Larsen et al., 2010). Error bars on red squares in **Figure 1b** result from the range of coefficients described here.

Sediment Aggradation Calculation

To determine distribution of sediment aggradation throughout the study area in the absence of post-Morakot elevation data, we outlined post-Morakot channels in Google Earth throughout each of the 15 studied drainage basins using the oldest available post-Morakot imagery, generally taken in the years 2009-2012. Overlaying these outlines on top of a pre-Morakot 5m resolution DEM, we extracted elevations along channel edges and fit a surface to the outline of post-Morakot channels using an inverse distance weighting function in ArcMap 10.5. The DEM

made from digitized and orthorectified aerial photographs during low-flow season. This surface represents the post-Morakot channel elevation, making the assumption that aggraded surfaces are relatively flat across channels. (**Figure S1**). Subtracting pre-storm elevation from this new surface produces maps of channel aggradation in each drainage basin (**Figure S2, Figure S3**). Error bars on blue diamonds in **Figure 1B** result from a $\pm$ 50cm error on the DEM used in this processing.

True error for this calculation is difficult to assess. One source of uncertainty is the potential for human inaccuracy in mapping channel boundaries, which is difficult to quantify as it has a greater impact in the steeper regions due to higher hillslope angle. Additionally, we are assuming by interpolating between channel boundaries that the geometry of the channel surfaces is near-horizontal, which is probably not strictly true. However, **Figure 1B** shows that trends in both landslide initiation and sediment aggradation covary over four orders of magnitude. It is unlikely that any unaccounted-for factors are enough to detract from the large-scale patterns of sediment release and aggradation in the study area. In **Table S4** we present some independent estimates of channel aggradation using simple hillslope geometry and find that our method predicts values that are similar to those estimated by simply measuring change in channel width and assuming planar hillslopes with representative angles.

Sediment Transport Model

To estimate the evacuation timeline of aggraded Morakot sediment, we model bedload sediment transport using grain size, daily water discharge, and channel morphology. Sediment grain size was determined using Wolman pebble counts of around 100 points at 36 locations across the study area (**Figure S4**). Our model of bedload sediment transport uses the range of

median grain sizes from all surveys within each drainage basin for which we have completed more than one survey. Some basins only have one survey, so there is only a single median value as reported in **Table S3**. Basins E1 and E10 do not have measured grain size data, so we use data from nearby W1 and E11, respectively. River discharge is available only for two basins within the study area. The Ailiao river basin (marked with white star in **Figure 1**), and the Chih-Pen river. Daily discharge is available at the Ailiao river mouth from 1964 to present. The record of discharge in the Chih-Pen is discontinuous and ends in 2015. To calculate sediment transport capacity in the other basins in the study area, we assume similar patterns of precipitation and runoff across the region and scale daily discharge linearly with drainage area using the discharge data from the Ailiao river (**Figure S5**). We estimate bedload sediment transport capacity at the mouth of each basin using an equation modified from Wong & Parker, 2006. Basal shear stress is calculated assuming a rectangular channel using the equation

$$\tau_b = (\rho g \frac{Q}{W * n})^{3/5} * S^{7/10}$$

Where ρ is density of water, g is acceleration from gravity, Q is water discharge scaled by drainage area, W is channel width, n is the Manning's friction factor (here we use a constant 0.065), and S is channel slope. Bedload transport capacity, Q_b, is calculated with the equation (Wong & Parker, 2006)

$$Q_b = 3.97\rho_s W(\frac{\tau_b}{(\rho_s - \rho)gD} - \tau_c)^{3/2} * D^{3/2}\sqrt{\frac{(\rho_s - \rho)}{\rho}g}$$

where ρ_s is the density of sediment (2650 kg/m^3), τ_c is the critical Shields stress (0.045), and D is a range of median grain sizes from all surveys in each basin. Bedload transport capacity is calculated using maximum daily discharge, and we use a range of ratios from 1/3 to 1/2

bedload to suspended sediment transport. Summing over all available gauging data since Typhoon Morakot, we estimate the total sediment transport since deposition of the landslide sediment (**Figure 3B**). The error reported in **Table S3** and **Figure 3B** is the combined effect of the range of grain sizes used and the range of bedload fractions used.

Most of the channels in this study area only reach bank full width during very large floods. For this reason, we allow for changing channel width by using a rating curve between channel width and discharge. **Figure S7** shows this relationship by plotting a linear trendline between log-transformed discharge and width data. The data for this rating curve was obtained from the location of the Sandimen river gauging station for the 11 dates since Typhoon Morakot for which both Google Earth aerial imagery and river discharge are available. We note that the power law exponent for this relationship, 0.26, is roughly comparable to that of Leopold and Maddock (1953).

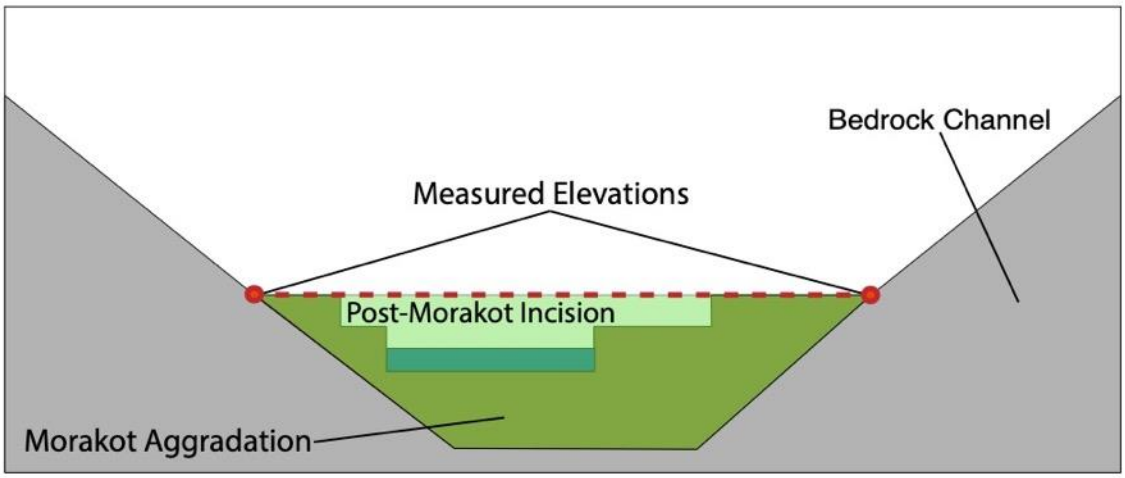

Figure S1. Schematic of channel aggradation measurement. Channel edge elevations (red circles) are used to make a plane representing the post-Morakot channel (red dashed line). Volume between this surface and pre-Morakot topography (grey) represents Morakot aggradation (green shaded).

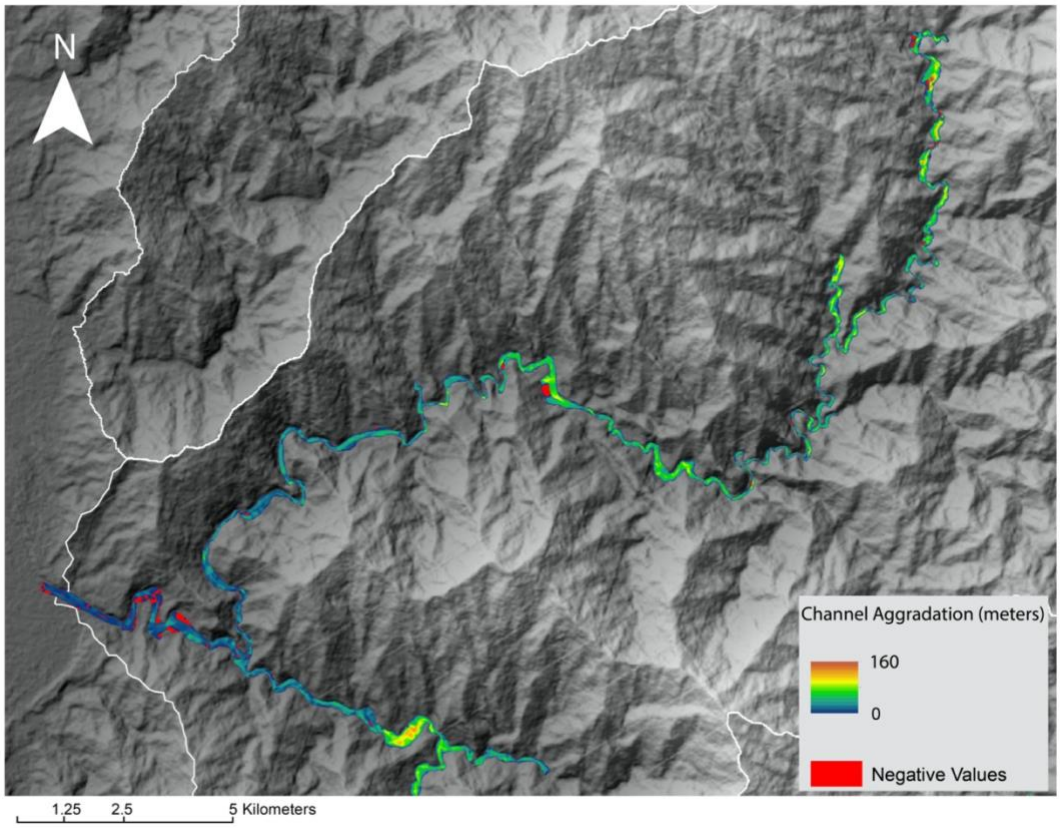

Figure S2. Mapped sediment aggradation in the Sandimen (W9) catchment.

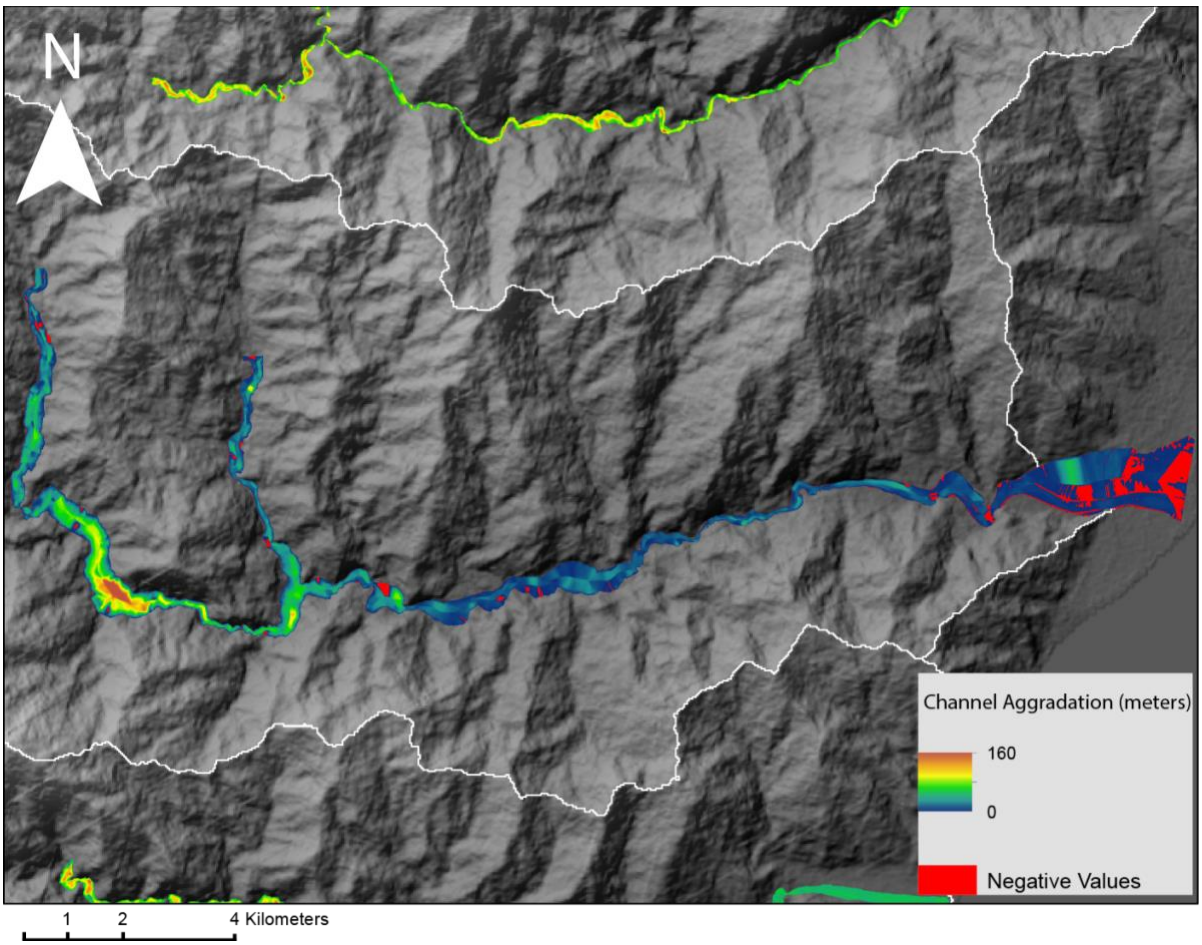

Figure S3. Mapped sediment aggradation in the Jinfeng (E9) catchment.

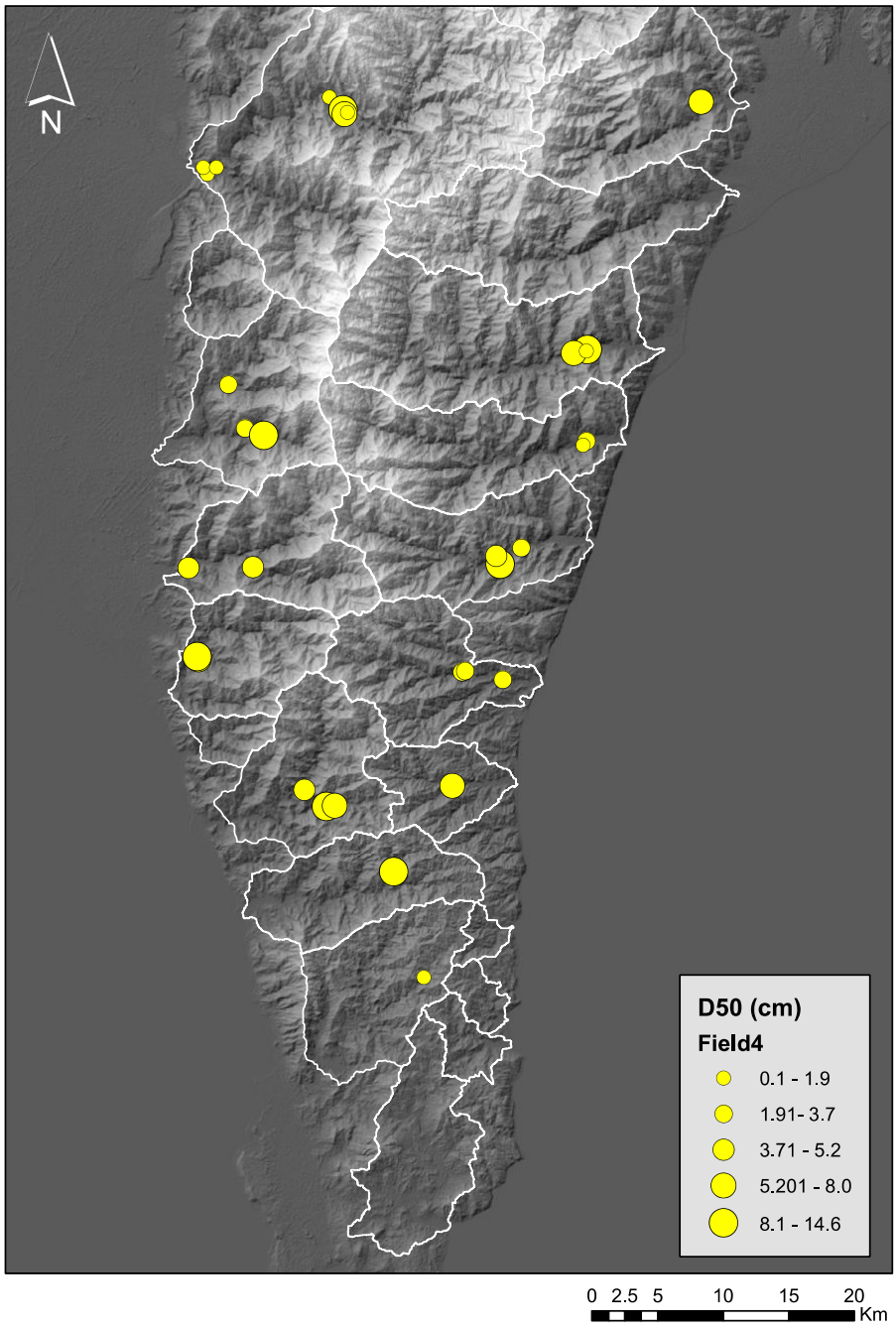

Figure S4. Locations of pebble counts. Markers are sized by median grain size measured along b-axis.

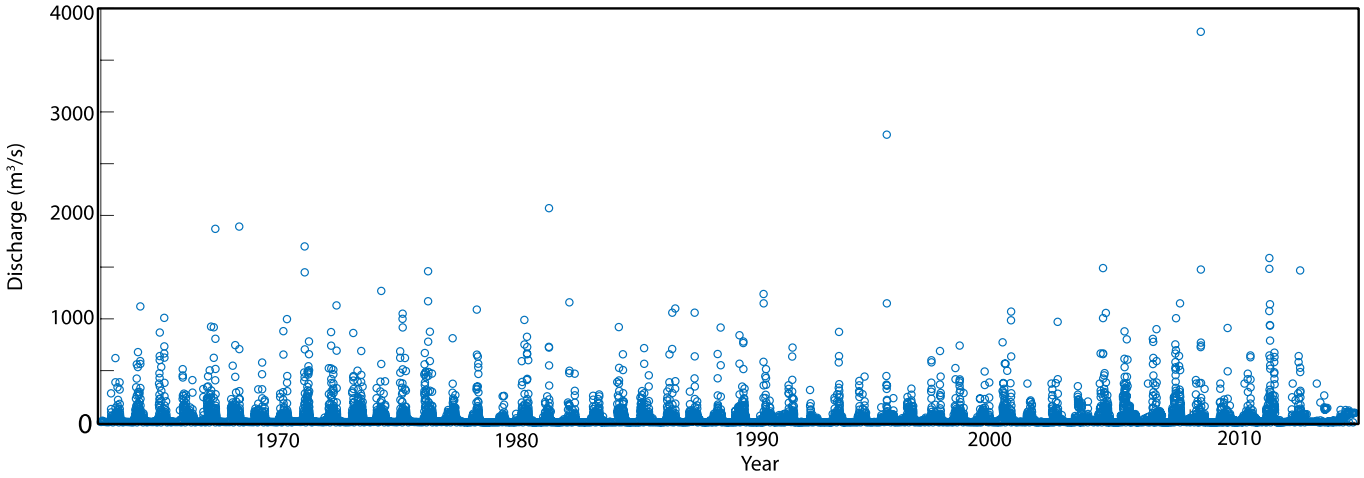

Figure S5. Time series of mean daily discharge data for the Ailiao river used in calculations of bedload sediment transport.

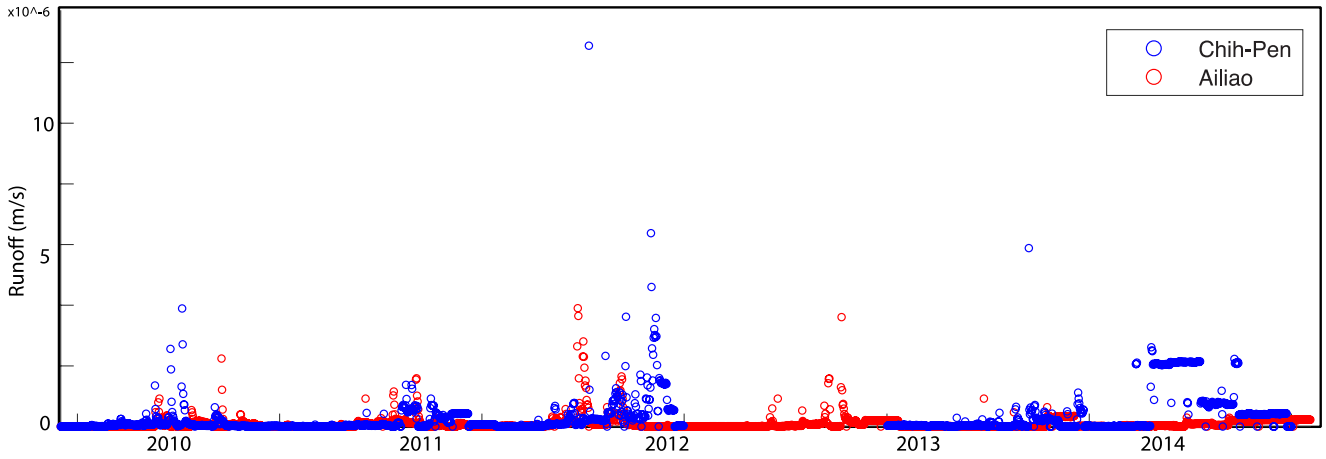

Figure S6. Time series of runoff values for both the Ailiao river and the Chih-Pen river in units of m/s. The mean difference in runoff for the dates at which data exists from both locations is $0.17*10^{-6}$ m/s.

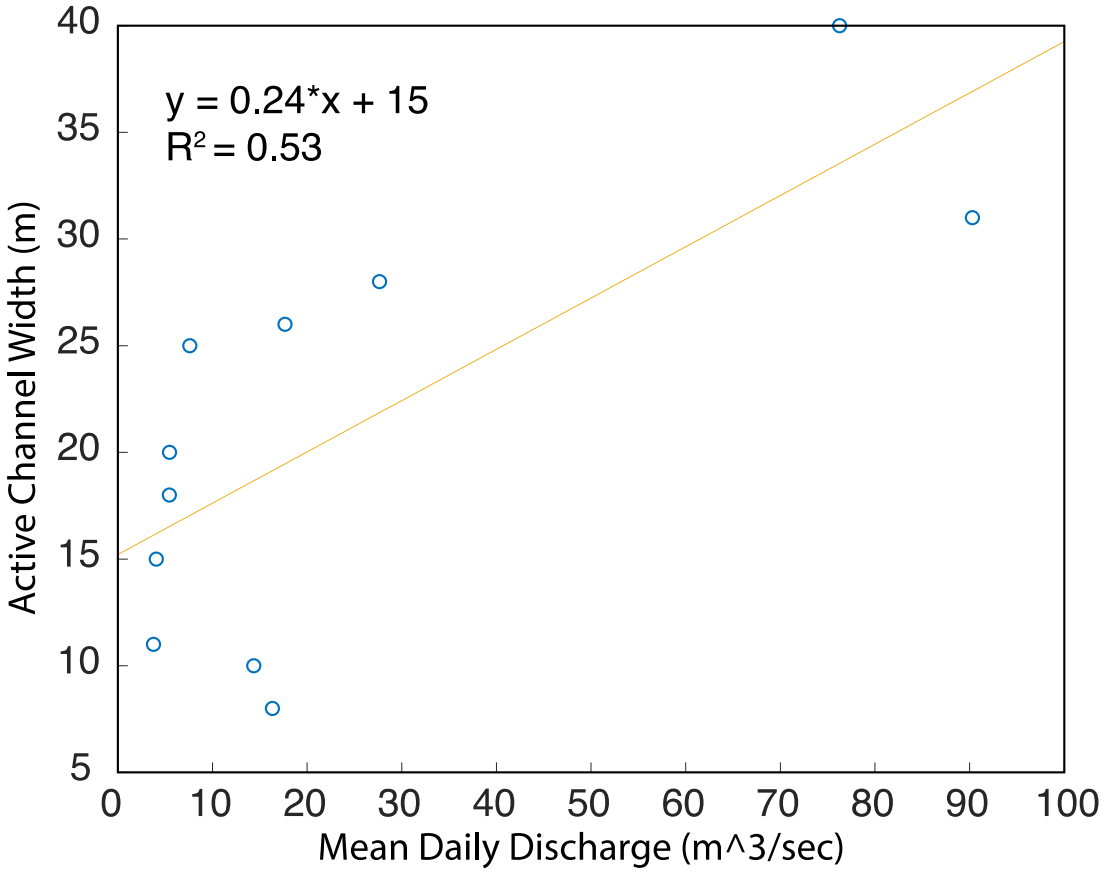

Figure S7. Rating curve used for estimation of channel width from discharge data. Channel width was measured from Google Earth imagery at the location of the Ailiao gauging station for the 11 dates exist since Typhoon Morakot for which both discharge and aerial imagery are available.

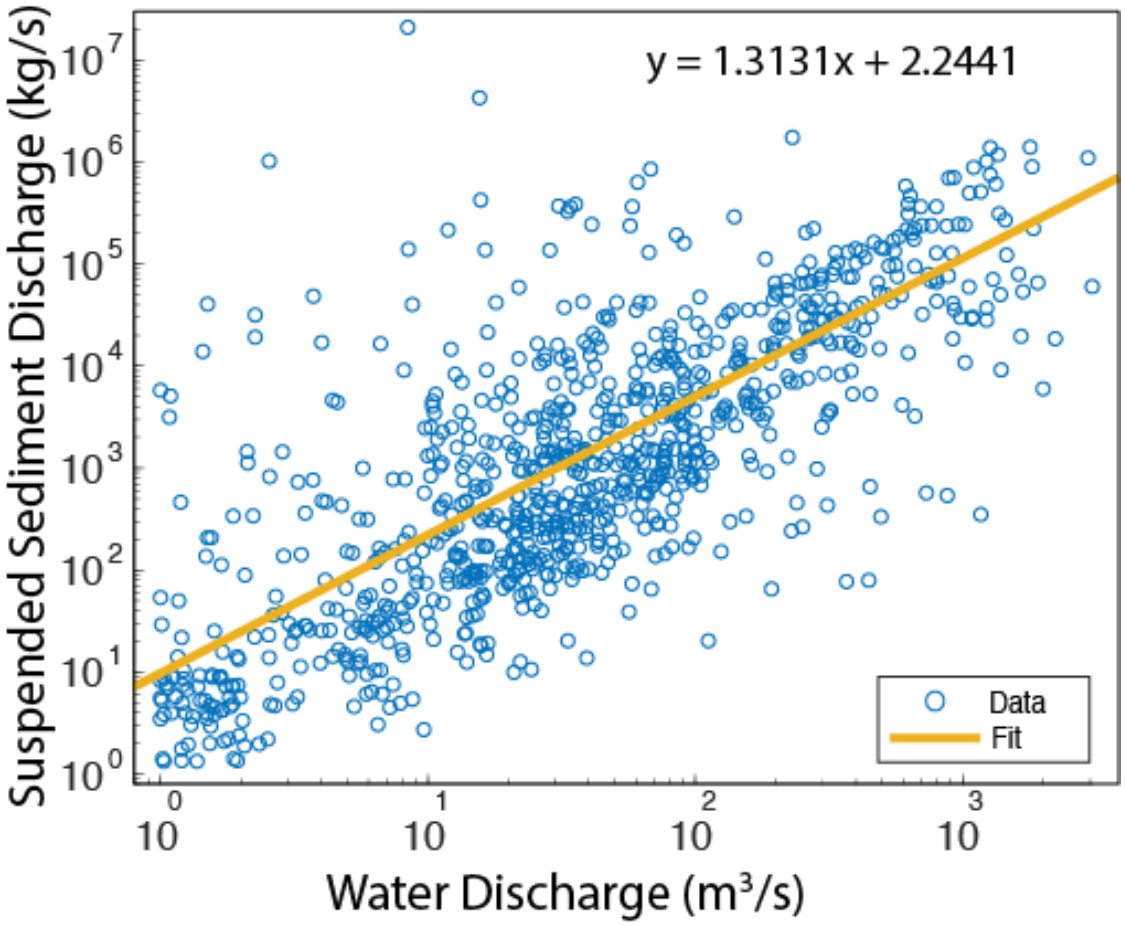

Figure S8. Sediment Rating curve used for estimation of suspended sediment discharge from river discharge. Gauging data began in 1964 at this location on the Sandimen River.

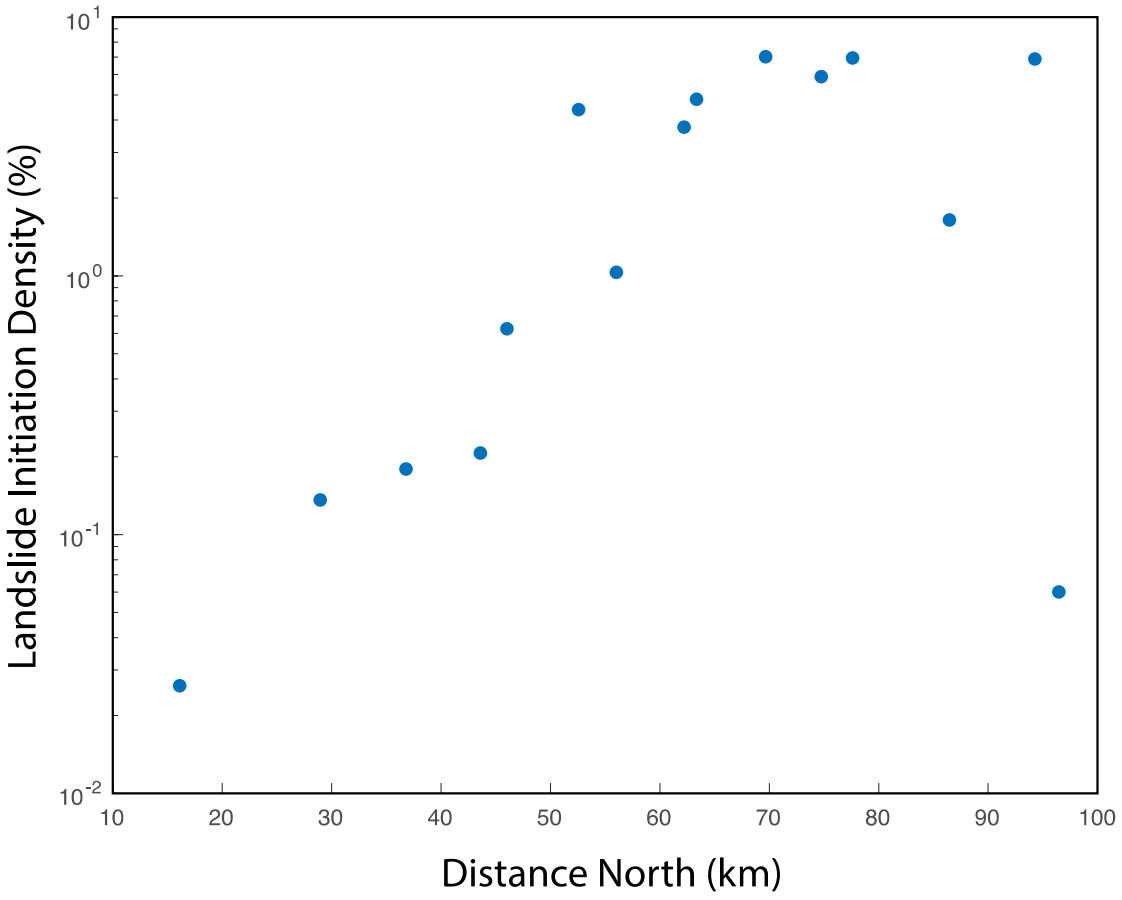

Figure S9. Gradient in percent of catchment impacted by landsliding across the study area. Each data point represents one drainage basin. X-axis is distance north of the southern tip of Taiwan. Y-axis is percentage of each drainage basin impacted by landslides on a logarithmic scale.

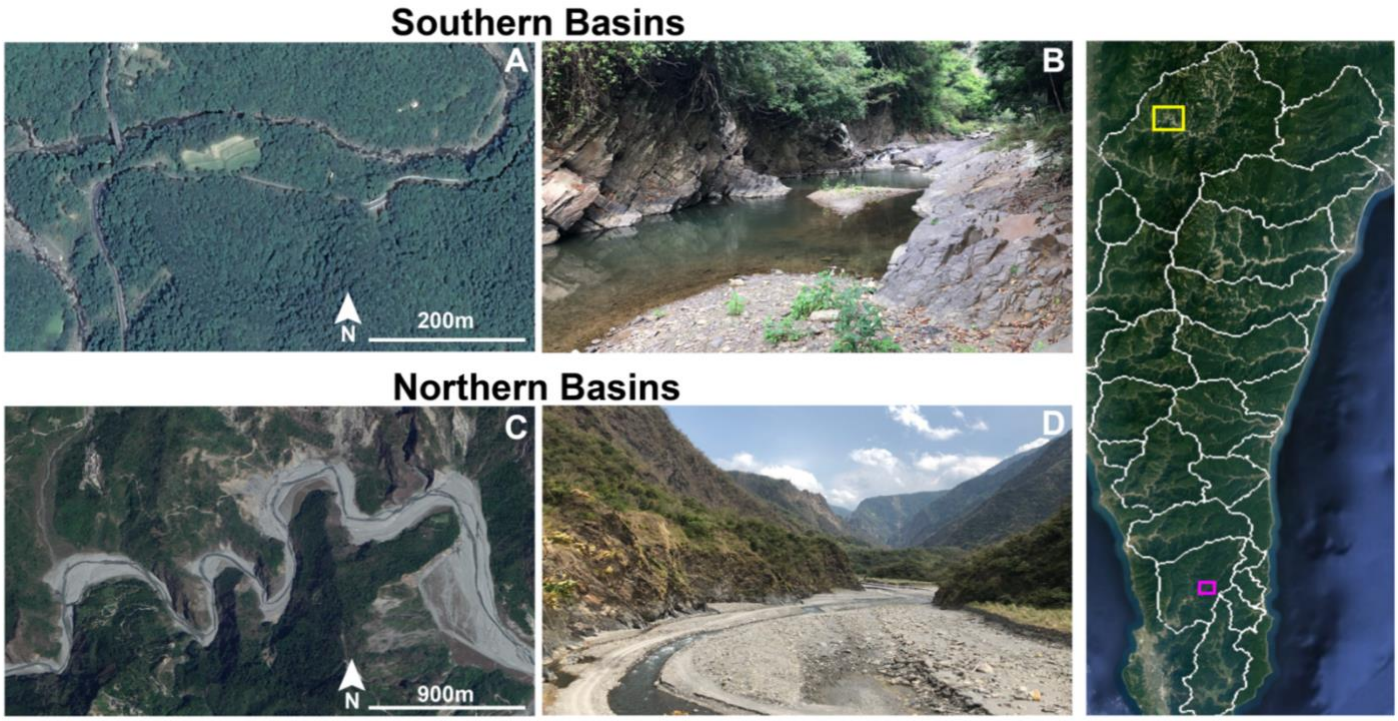

Figure S10. Differences in sediment cover between rivers in southern and northern drainage basins. A) Google Earth image of the river in Mudan drainage basin (W1). B) Photograph of river in Mudan drainage basin. Note the narrow channel with widespread bedrock exposure. C) Google Earth image of river in Ailiao drainage basin (W9). D) Photograph of river in Ailiao drainage basin. Channel here is very wide, and completely covered with sediment. Note the difference in sclaes between A and C. Map on right shows locations of A and B (pink box) and C and D (yellow box).

Figure S11. Example of time evolution of Morakot aggradation surface. Sediment is deposited during the 2009 typhoon Morakot. By 2019 a fill terrace has been abandoned, but the latest imagery shows that this surface is rapidly retreating and is likely to all be mobilized. Located in the Ailiao river (basin W9) at 267718m E, 2519189m N. UTM 51Q.

Table S1. Data regarding basin area, landslide area and volume, and channel aggradation for all studied catchments. Error on landslide volume calculation is the result of the range of coefficients presented in Larsen & Montgomery, 2012. This range also determines error in single-event hillslope denudation. Error on aggraded channel volume calculation is the result of the ±50cm vertical error of the 5m Taiwanese DEM from which these data were collected.

Basin Name	Distance From Southern Tip of Taiwan (km)	Basin Area (km^2)	Landslide Area (km^2)	Landslide Initiation Density (% Basin Area)	Landslide Volume (km^3)	Aggraded Channel Volume (km^3)	Average Single Event Hillslope Erosion (mm)
W1	28.97	114.52	0.1560	0.14	0.0005 ± 0.0001	0.0008 ± 0.0007	4 ± 1.1
W2	36.80	102.55	0.1839	0.18	0.0004 ± 0.0001	0.0026 ± 0.002	4 ± 1.1
W3	46.03	120.04	0.7499	0.62	0.0022 ± 0.0006	0.0060 ± 0.003	18 ± 5.1
W5	56.03	86.95	0.8976	1.03	0.0027 ± 0.0008	0.0025 ± 0.0009	32 ± 9.0
W6	63.35	116.58	5.6139	4.82	0.0277 ± 0.009	0.0277 ± 0.003	238 ± 78.8
W7	74.75	125.42	7.3826	5.89	0.0467 ± 0.02	0.0192 ± 0.003	372 ± 131.9
W9	94.27	406.82	28.0260	6.89	0.1051 ± 0.03	0.1282 ± 0.009	258 ± 80.3
E1	16.12	100.65	0.0262	0.03	0.00006 ± 0.00002	0.0005 ± 0.0005	1 ± 0.2
E5	43.60	55.26	0.1141	0.21	0.0004 ± 0.0001	0.00002 ± 0.0005	7 ± 2.1
E6	52.57	109.79	4.8190	4.39	0.0286 ± 0.01	0.0196 ± 0.004	260 ± 91.1
E7	62.22	133.93	5.0265	3.75	0.0246 ± 0.008	0.0204 ± 0.004	184 ± 59.5
E8	69.66	150.35	10.5630	7.03	0.0464 ± 0.01	0.0469 ± 0.004	309 ± 95.6
E9	77.61	211.92	14.7220	6.95	0.0978 ± 0.03	0.1838 ± 0.01	461 ± 162.3
E10	86.46	173.41	2.8502	1.64	0.0094 ± 0.003	0.0179 ± 0.003	54 ± 15.7
E11	96.46	147.73	0.0887	0.06	0.0002 ± 0.00006	0.0031 ± 0.002	1 ± 0.4

Table S2. Data from Wolman pebble count surveys. D_{16}, D_{50}, and D_{84} are the 16th, 50th, and 84th percentile of grain size respectively. Each survey consists of measurements gathered along one or more transects at equal spacing. Measurements were taken every meter. All grains measured along b-axis. Row n is the number of measurements in each survey. Date listed is the one on which the survey was completed.

Survey	1	2	3	4	5	6	7	8
Date	3/10/18	3/11/18	3/12/18	3/13/18	3/14/18	3/14/18	3/14/18	3/15/18
Latitude	22.7086	22.7630	22.5290	22.4383	22.3639	22.4545	22.5287	22.5260
Longitude	120.6546	120.7446	120.6992	120.6456	120.8791	120.8915	120.9387	120.9363
n	102	98	102	102	102	102	102	102
D_{84} (cm)	10.2	6.6	23.1	7.5	8.6	11.0	11.0	8.3
D_{50} (cm)	0.95	0.55	4.6	0.7	2.15	3.25	3.55	0.10
D_{16} (cm)	0.01	0.01	0.8	0.05	0.09	0.1	0.05	0.05

Survey	9	10	11	12	13	14	15	16
Date	3/6/19	3/6/19	3/7/19	3/8/19	3/8/19	3/8/19	3/8/19	3/9/19
Latitude	22.5340	22.5642	22.3747	22.7631	22.7545	22.7515	22.7528	22.7133
Longitude	120.6856	120.6727	120.6539	120.7444	120.7547	120.7559	120.7580	120.6517
n	100	100	100	100	100	101	100	100
D_{84} (cm)	12.2	14.8	17.0	6.8	38.3	40.1	13.1	11.5
D_{50} (cm)	3.7	3.5	8.0	1.2	14.6	6.3	0.25	1.05
D_{16} (cm)	0.9	0.2	2.6	0.1	1.1	0.8	0.1	0.1

Survey	17	18	19	20	21	22	23	24
Date	3/9/19	3/10/19	3/10/19	3/11/19	3/11/19	3/12/19	3/12/19	3/13/19
Latitude	22.7515	22.2748	22.2860	22.2306	22.2901	22.4431	22.4489	22.5920
Longitude	120.7559	120.7501	120.7335	120.8005	120.8430	120.8762	120.8731	120.9386
n	100	97	100	110	100	100	100	100
D_{84} (cm)	8.9	48.9	18.0	44.9	18.9	56.0	13.5	32.5
D_{50} (cm)	0.2	10.8	5.0	12.4	7.45	11.65	4.15	10.35
D_{16} (cm)	0.1	1.6	1.4	1.4	2.8	1.7	0.2	0.2

Survey	25	26	27	28	29	30	31	32
Date	3/13/19	3/13/19	3/14/19	3/3/20	3/3/20	3/4/20	3/4/20	3/5/20
Latitude	22.5896	22.7635	22.1582	22.5908	22.5922	22.3686	22.3695	22.2753
Longitude	120.9283	121.0205	120.8241	120.9378	120.9364	120.8490	120.8513	120.7563
n	100	104	100	100	100	100	100	100
D_{84} (cm)	16.1	36.5	6.5	29.0	10.4	7.0	10.6	32.0
D_{50} (cm)	6.55	7.05	1.9	0.2	3.4	3.1	3.7	5.9
D_{16} (cm)	0.1	0.2	1.0	0.1	0.7	1.2	0.2	1.7

Survey	33	34	35	36
Date	3/6/20	3/6/20	3/6/20	3/7/20
Latitude	22.3765	22.4375	22.4387	22.5296
Longitude	120.6527	120.6454	120.6929	120.6996
n	100	100	100	95
D_{84} (cm)	21.0	12.5	26.7	41.5
D_{50} (cm)	12.0	4.6	5.2	13.0
D_{16} (cm)	3.6	1.8	0.55	1.9

Table S3. Data regarding sediment transport inputs and results. Final column is calculated as the ratio of modeled sediment transport capacity to sediment aggradation from Typhoon Morakot, multiplied by 100. The smallest of these values (6 ± 1) indicates an estimated removal of 5-7% of aggraded sediment, while the largest (2033 ± 1598) indicates a sediment transport capacity many times larger than the volume of aggraded sediment.

Basin Label	**Minimum D_{50} (cm)**	**Maximum D_{50} (cm)**	**Channel Width at Mouth (m)**	**Channel Gradient at mouth**	**Cumulative Sediment Flux 8/11/2009 to 12/31/2019(m^3)**	**Percent of Morakot Sediment Mobilized**
W1	1.9	1.9	64.4	0.045	1.5e6 ± 3.0e5	191 ± 140
W2	12.4	12.4	95.3	0.045	2.1e6 ± 4.3e5	83 ± 44
W3	5.0	10.8	279.0	0.045	6.7e6 ± 1.3e5	112 ± 55
W5	8.0	12.0	156.2	0.045	3.3e6 ± 6.5e5	133 ± 51
W6	0.7	5.2	184.1	0.045	4.4e6 ± 8.7e5	16 ± 4
W7	3.5	13.0	121.1	0.052	3.4e6 ± 6.7e5	18 ± 5
W9	0.2	14.6	166.8	0.056	7.8e6 ± 1.5e6	6 ± 1
E1	1.9	1.9	171.2	0.012	9.7e5 ± 1.9e5	193 ± 172
E5	7.5	7.5	91.6	0.012	4.1e5 ± 8.1e4	2033 ± 159
E6	2.2	3.7	241.8	0.024	2.9e6 ± 5.8e5	15 ± 5
E7	3.3	11.7	188.2	0.032	3.3e6 ± 6.3e5	16± 5
E8	0.1	3.6	262.8	0.036	5.5e6 ± 1.1e6	12 ± 3
E9	0.2	10.4	284.1	0.099	1.9e7 ± 3.8e6	10 ± 2
E10	7.1	7.1	203.5	0.099	1.3e7 ± 2.6e6	72 ± 20
E11	7.1	7.1	113.6	0.099	6.7e6 ± 1.4e6	218 ± 145

Table S4. Comparing measured aggradation with estimates of aggradation using simple geometric calculations in order to loosely validate mapped aggradation. Channel width change is the difference in pre- and post-Morakot channel widths. Aggradation estimates are calculated as one half of the width change divided by the tangent of 90º minus the hillslope angle. We are assuming planar hillslopes and using minimum and maximum values of 30º and 45º, a reasonable range for our study area. Locations are in UTM 51Q. There is clearly some inaccuracy to this test, but most measured locations fall near or within the range of estimates.

Easting (m)	Northing (m)	Channel Width Change (m)	Measured Aggradation (m)	Aggradation Estimate with 30º slopes (m)	Aggradation Estimate with 45º slopes (m)
275135	2499608	400	165	115	200
267718	2519189	82	27	24	41
265407	2510775	300	60	86	150
281546	2491488	124	35	36	62

References

Larsen, I. J., Montgomery, D. R., & Korup, O. (2010). Landslide erosion controlled by hillslope material. *Nature Geoscience*, *3*(4), 247-251.

Leopold, L. B., & Maddock, T. (1953). *The hydraulic geometry of stream channels and some physiographic implications* (Vol. 252). US Government Printing Office.

Marc, O., Stumpf, A., Malet, J. P., Gosset, M., Uchida, T., & Chiang, S. H. (2018). Initial insights from a global database of rainfall-induced landslide inventories: The weak influence of slope and strong influence of total storm rainfall. *Earth Surface Dynamics*, *6*(4), 903-922.

Wong, M., & Parker, G. (2006). Reanalysis and correction of bed-load relation of Meyer-Peter and Müller using their own database. *Journal of hydraulic engineering*, *132*(11), 1159-1168.